The Electrocatalytic Oxygen Evolution Reaction Activity of Rationally Designed NiFe-Based Glycerates

Vivek Kumar Singh,[1#] Bibhudatta Malik,[1#] Rajashree Konar, [1] Efrat Shawat Avraham, [1] and Gilbert Daniel Nessim *,[1]

[1] Department of Chemistry, Bar Ilan Institute for Nanotechnology and Advanced Materials (BINA), Bar Ilan University, 52900, Ramat Gan, Israel;
vivekkumarsingh.rs.cer18@itbhu.ac.in (V.K.S.); malikbi@biu.ac.il (B.M.);
rajashree.konar@biu.ac.il (R.K.); epale086@gmail.com (E.S.A.)

 # Authors contributed equally

*** Corresponding author Email: gdnessim@biu.ac.il**

Synthesis of nickel iron layered double hydroxide (NiFe LDH): Nickel iron layered double hydroxide (NiFe LDH) was synthesised by the one-pot hydrothermal process. In this typical procedure, 3 mM nickel (II) nitrate hexahydrate (98%), 1 mM iron (III) nitrate nonahydrate (98%), 4 mM urea (CH_4N_2O, 99%) and 6 mM ammonium fluoride (NH_4F, 98%) were dissolved in 30 ml of deionized water (DI) water and stirring for the 20 minutes at 500 rpm to get the homogeneous solution after that the solution was transferred to the 50 ml Teflon-lined stainless-steel autoclave and kept at 120 °C for 7 hours. Finally, the nickel iron layered double hydroxide (NiFe LDH) was separated by centrifugation and three times with washed deionized water (DI) and absolute ethanol and dried in a vacuum oven at 80 °C for 12 hours.

Material characterization: The as-synthesized different molar ratios of NiFeG powder samples were characterized using Powder X-ray diffraction (PXRD) (Bruker D8 (Billerica, MA, USA) advance under conditions of 40 kV and 44 mA with Cu Kα radiation (λ = 1.5418 Å). The infrared spectra of the samples were obtained by using a Fourier transform infrared spectroscopy (FTIR) spectrometer (Nicolet iS10), and spectra ranging from 4000 to 400 cm^{-1} were acquired. The morphology and structure of the samples were analyzed by using a high-resolution scanning electron microscope (HR-SEM) equipped with an energy-dispersive spectrometer (EDS) (FEI, Magellan 400L, Hillsboro, OR, USA). Transmission electron microscopy (TEM) (JEOL JEM-2100, Tokyo, Japan) was used to analyze the morphology and structure of as-synthesized samples. Before the TEM analysis, we dispersed as-synthesized NiFeG powder in 5 mL absolute ethanol

and bath sonicate for 2 min. and then drop-casted a drop of solution onto carbon coated Cu grid (300 mesh) and kept it for drying at ambient conditions. The Kratos axis HS spectrometer (Kratos, San Diego, CA, USA), combined with monochromatic (Al) and dual (Mg/Al) sources, was utilized for the XPS analysis.

Electrochemical characterizations:

We studied the OER performances of the prepared catalysts in a Biologic, VSP-128 potentiostat. A three-electrode setup was used in the study, working, reference, and counter electrodes used as glassy carbon electrode (GCE), Hg/HgO filled with 1M NaOH, and platinum spiral, respectively. The catalyst activation was carried out using cyclic voltammetry (CV) in the potential range of 1 to 1.3 V *Vs.* RHE for about 25 cycles at a scan rate of 50 mV/s. Further, the *I-V* polarization was done by subjecting 50 CV cycles (1-1.75 V *Vs.* RHE) at the scan rate of 50 mV/s to get stability. In this study, the potential at the reversible hydrogen electrode scale is calculated by $E_{RHE} = E_{Hg/HgO} + 0.935$ V, where the overpotential (η) can be found as $\eta = E_{RHE} - 1.23$ V. The double layer capacitance (C_{dl}) for the catalysts has been tested using CVs performed at non-faradic regions with sweep rates of 10-80 mV/s. The slope between charging current, I_c *Vs.* Scan rate provides C_{dl} value, which later has been used for ECSA calculation.

Working electrode preparation: 5 mg of the catalyst (powder) added to a homogenous solution of 700 µL DI H_2O, 250 µL of isopropanol, and 50 µL of the Nafion solution (5 wt %) and then dispersed under ultrasonication for 30 minutes. The obtained homogeneous catalyst ink of 5 µL was then drop costed over the 3 mm dia. GCE and kept for drying fully at room temperature for about 3 hours before the start of electrochemical measurements.

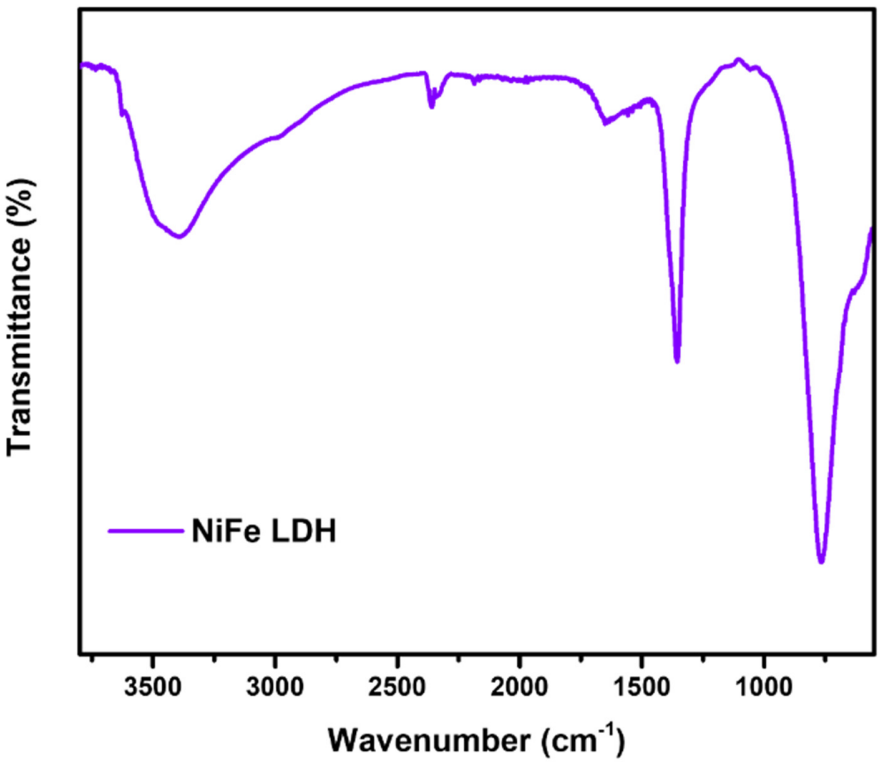

Figure S1: *Fourier transform infrared spectroscopy (FTIR) Spectrum of NiFe LDH Sample.*

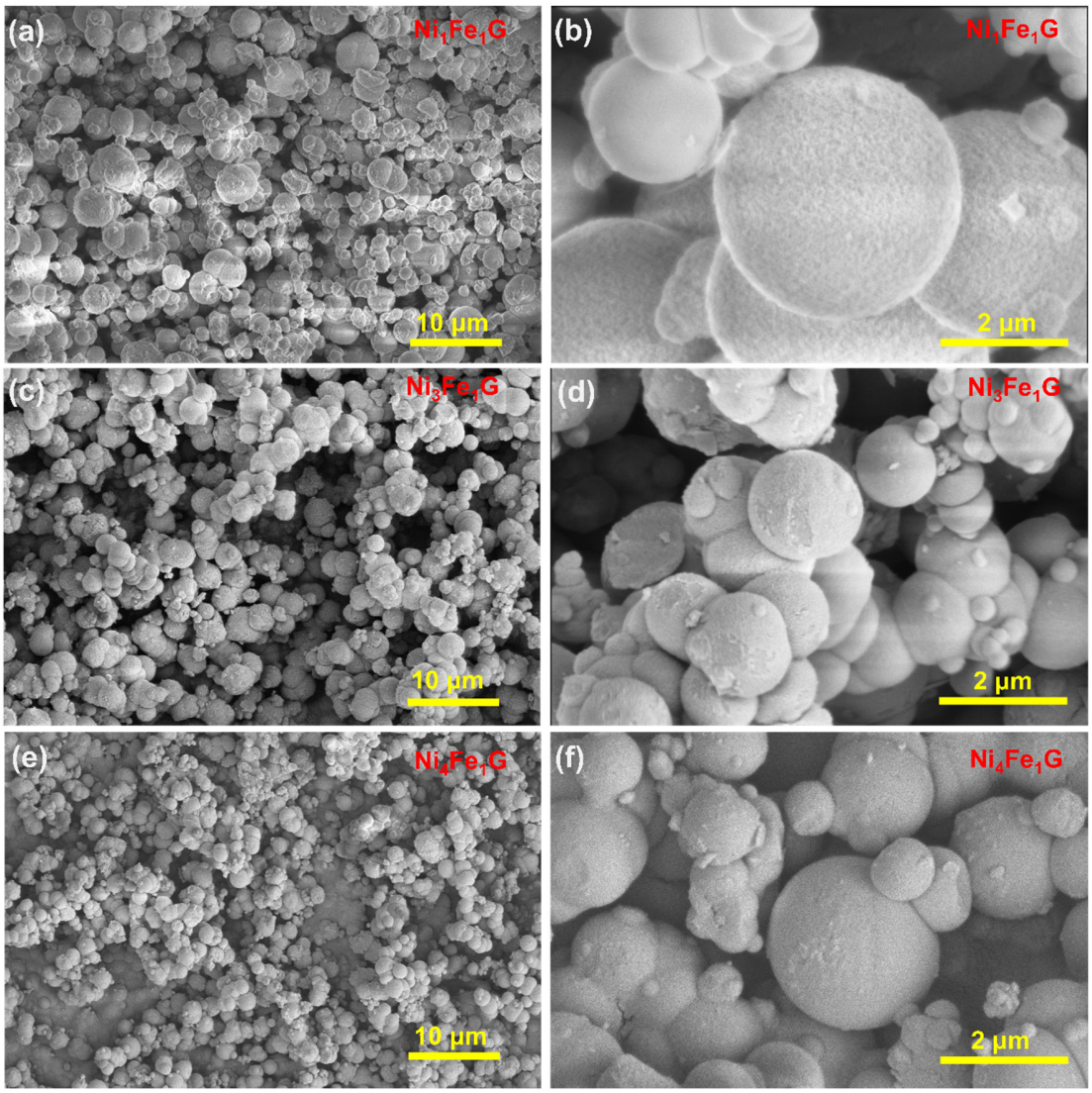

Figure S2: *SEM images of nickel iron glycerate (NiFeG) samples with different magnifications (a,b) Ni_1Fe_1G, (c,d) Ni_3Fe_1G, and (e,f) Ni_4Fe_1G*

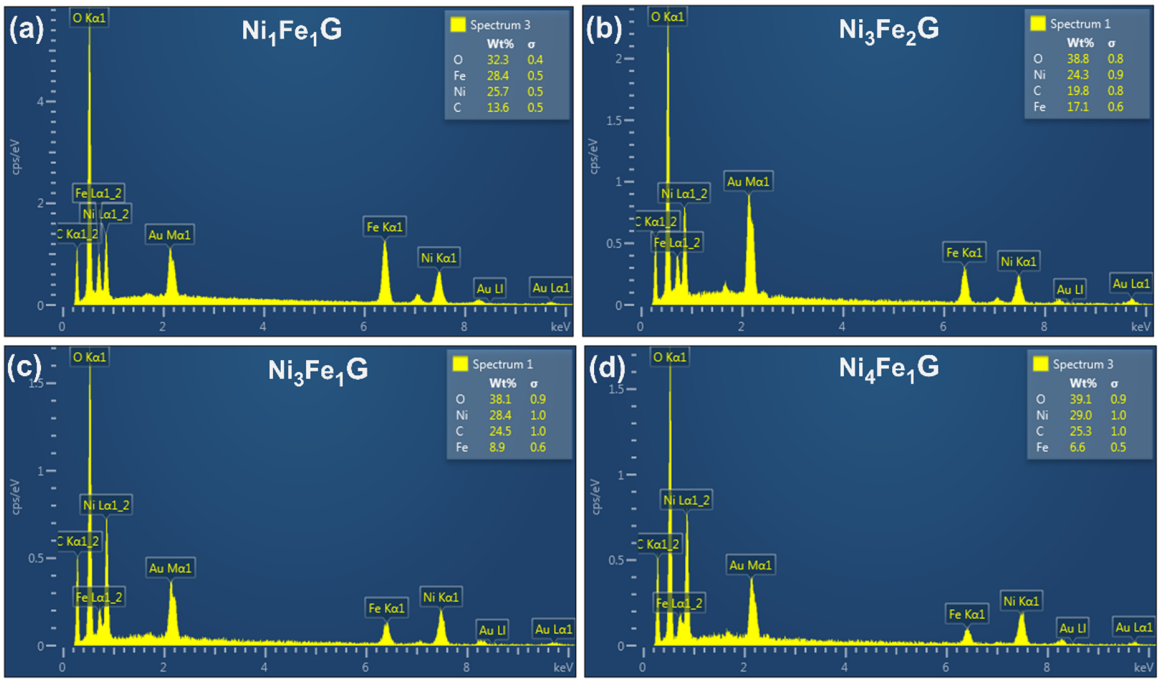

Figure S3: *Energy dispersive spectroscopy (EDS) of different ratios of NiFeG sample (1:1, 3:2, 3:1, and 4:1) showing the Ni, Fe, O, and C elements exist in the NiFeG sample.*

Table S1: *Illustrates the SEM-EDS elemental distributions of the different NiFeG samples.*

Samples	Ni Wt %	Fe Wt %	O Wt %	C Wt%	Ni:Fe ratio
Ni_1Fe_1	25.7	28.4	32.3	13.6	1:1
Ni_3Fe_2	24.3	17.1	38.8	19.8	3:2
Ni_3Fe_1	28.4	8.9	38.1	24.5	3.19:1 (3:1)
Ni_4Fe_1	29	6.6	39.1	25.3	4.3:1 (4:1)

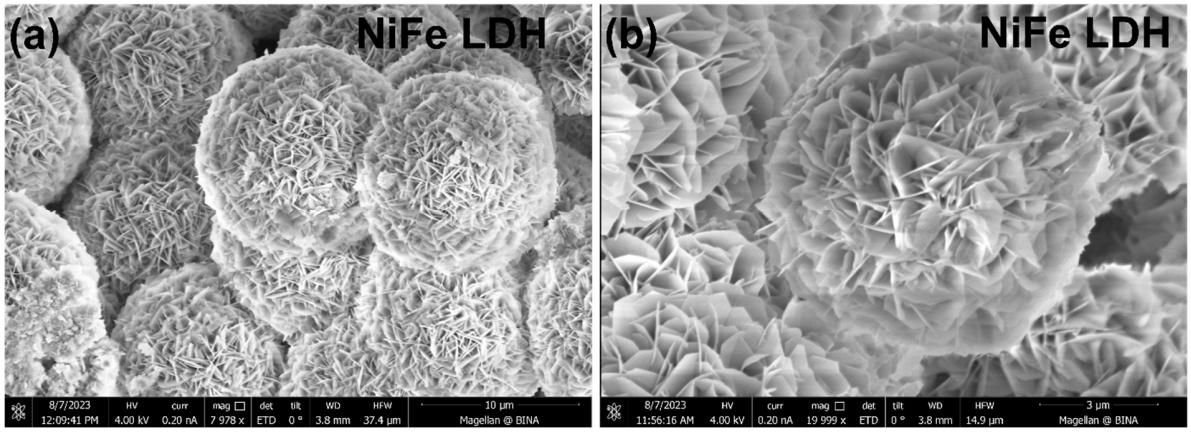

Figure S4: *(a & b) Show the FESEM image of the NiFe LDH synthesis by the one step hydrothermal process, which shows the flaky 2D structure with the sharp edges.*

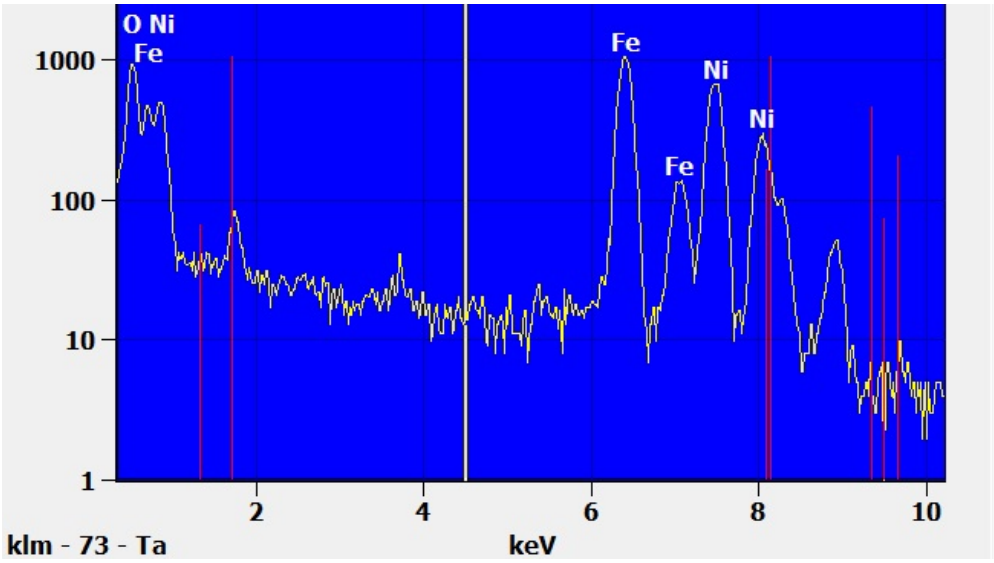

Figure S5: TEM EDX of Ni_3Fe_2G sample.

Table S2: *Illustrates the elemental distributions of Ni_3Fe_2G sample.*

Elements	Elements Wt%	Atomic %
C K	-	-
O K	26.24	55.92
Fe K	42.02	25.65
Ni K	31.74	18.43

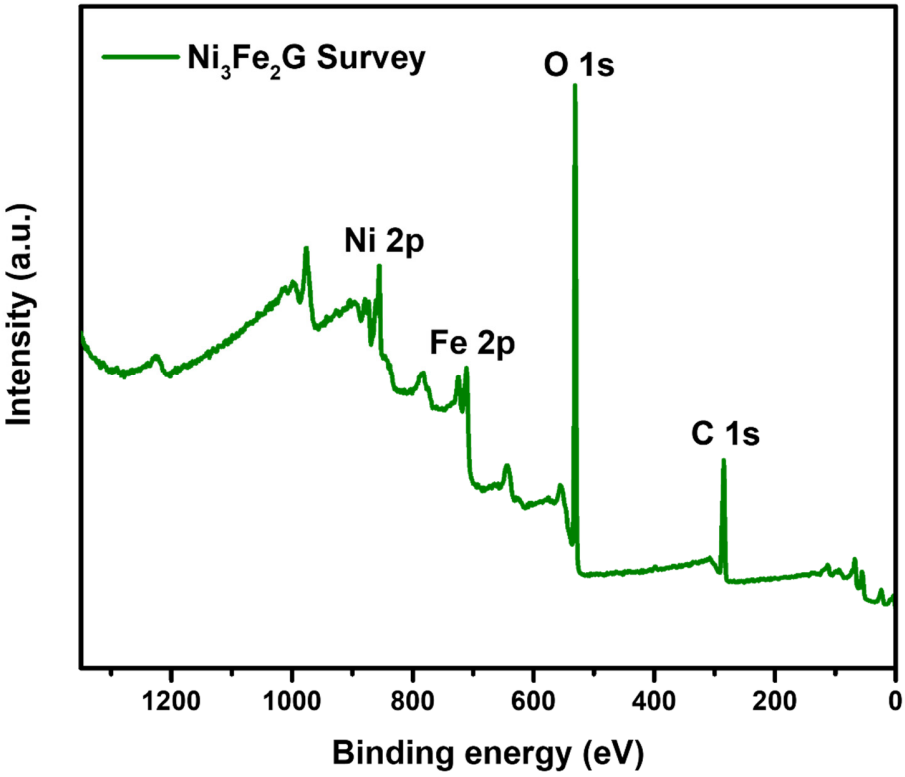

Figure S6: *XPS survey of Ni_3Fe_2G sample.*

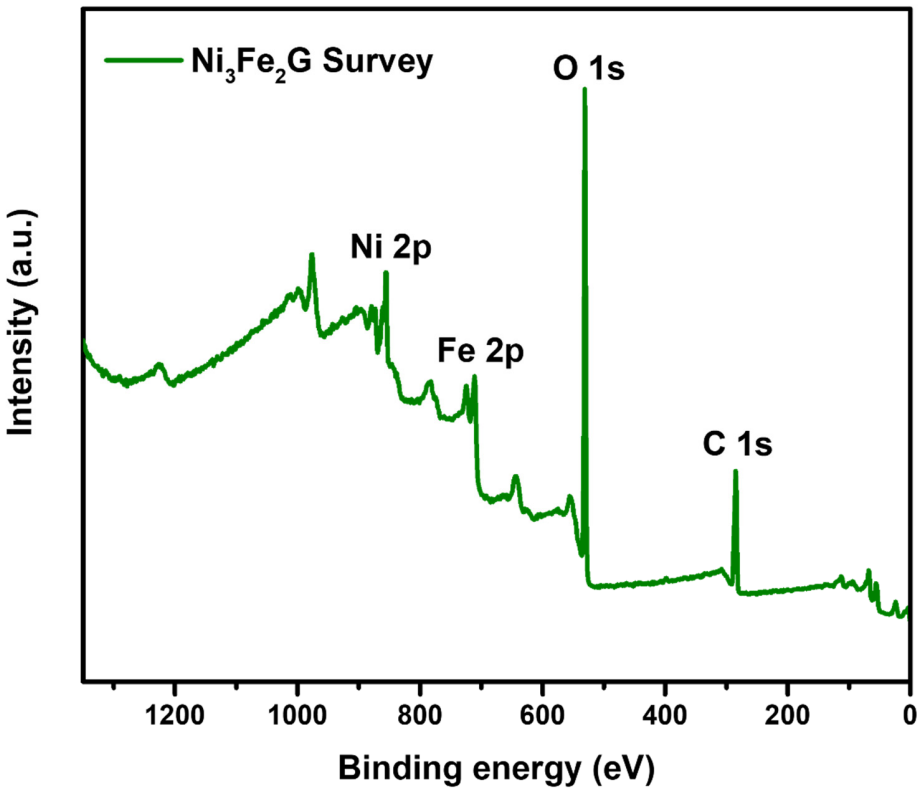

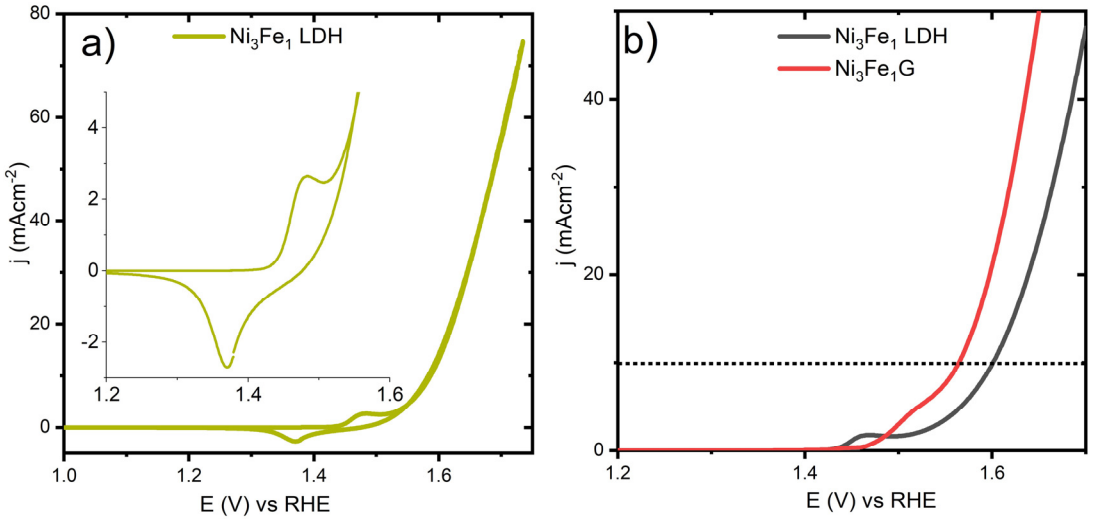

Figure S7: *(a) OER CV of NiFe LDH (inset shows the zoomed redox curve) and (b) LSV comparison of Ni_3Fe_1G and Ni_3Fe_1 LDH carried out at 5 mVs^{-1}.*

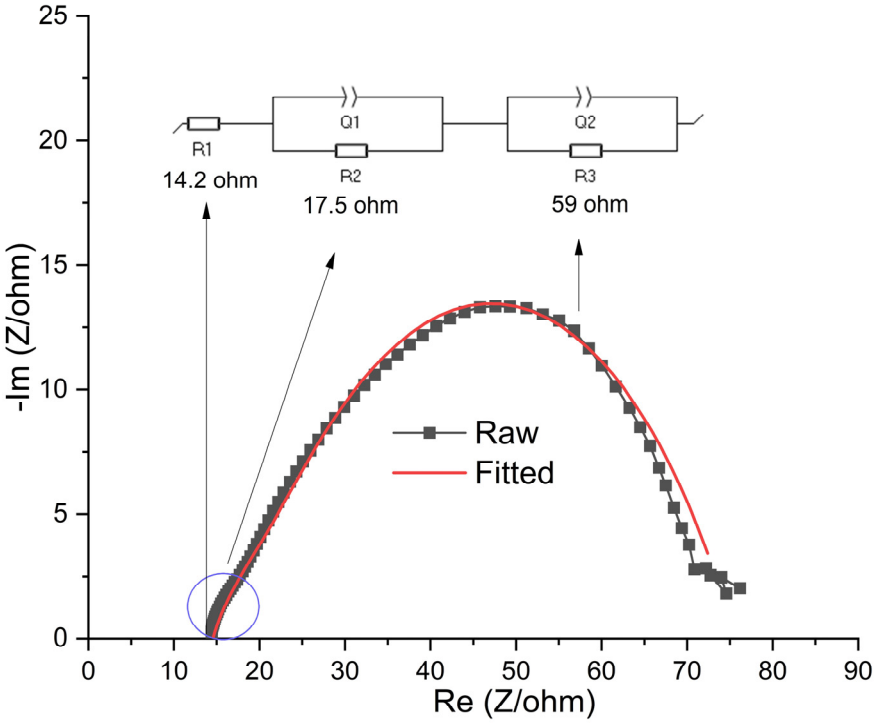

Figure S8: *Experimental and fitted EIS spectra of Ni_3Fe_1G (inset stands for the equivalent circuit diagram).*

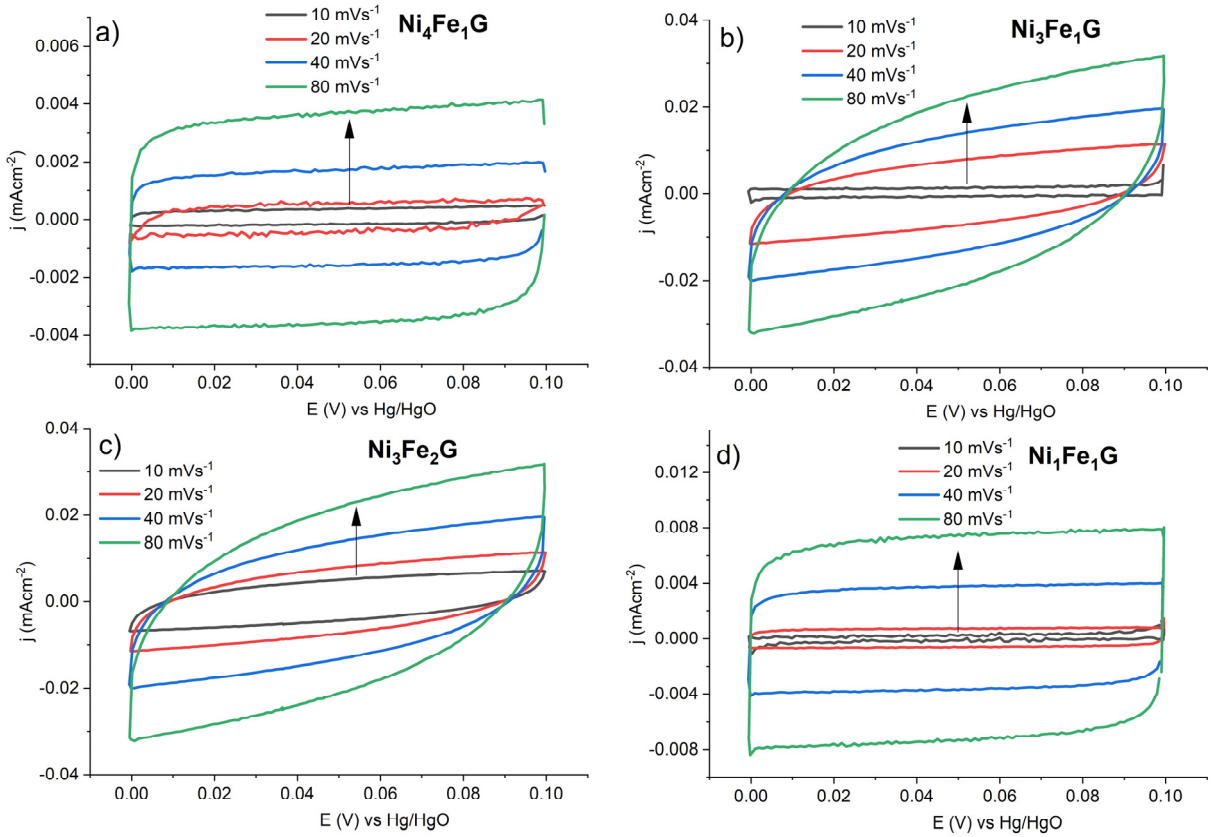

Figure S9: *CVs that carried out at various scan rates that stand for (a) Ni_4Fe_1G, (b) Ni_3Fe_1G, (c) Ni_3Fe_2G, and (d) Ni_1Fe_1G.*

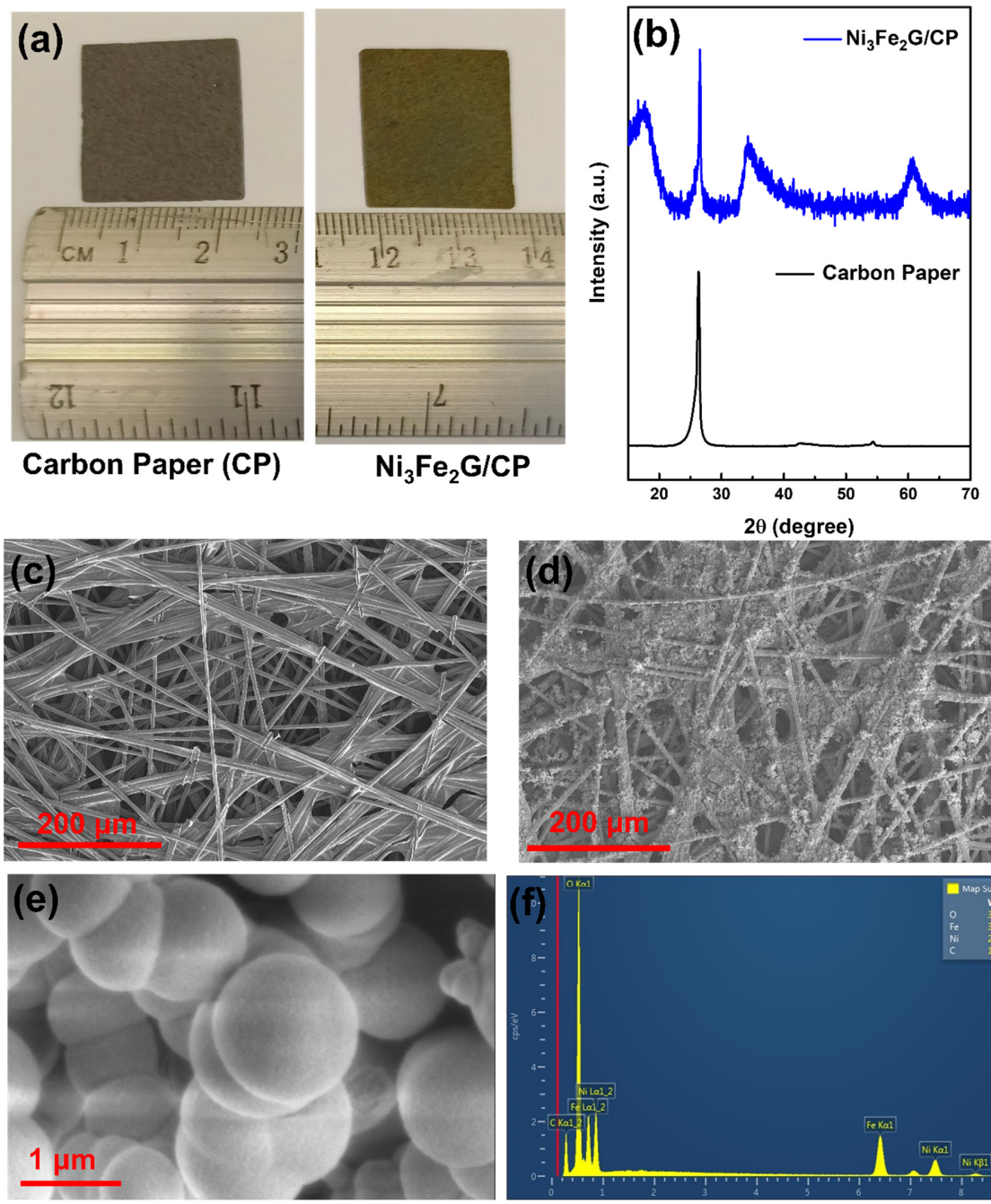

Figure S10: *(a) Show the images of pristine carbon paper (CP) and Ni₃Fe₂G microspheres grown on CP after the solvothermal synthesis, (b) comparative XRD pattern of the CP and Ni₃Fe₂G/CP, which show the typical diffraction peaks observed at 17.45°, 34.56°, and 60°.81°, indicating the formation of bimetallic glycerates (NiFeG). The diffraction peaks at 26.53° correspond to the CP,*

which is used as the substrate for the solvothermal synthesis of Ni_3Fe_2G on the surface of CP, (c) shows the SEM images of pristine CP, (d, e) SEM images of Ni_3Fe_2G microsphere at different magnifications, (f) Energy dispersive spectroscopy of Ni_3Fe_2G showing the existence of Ni, Fe, O, and C elements.

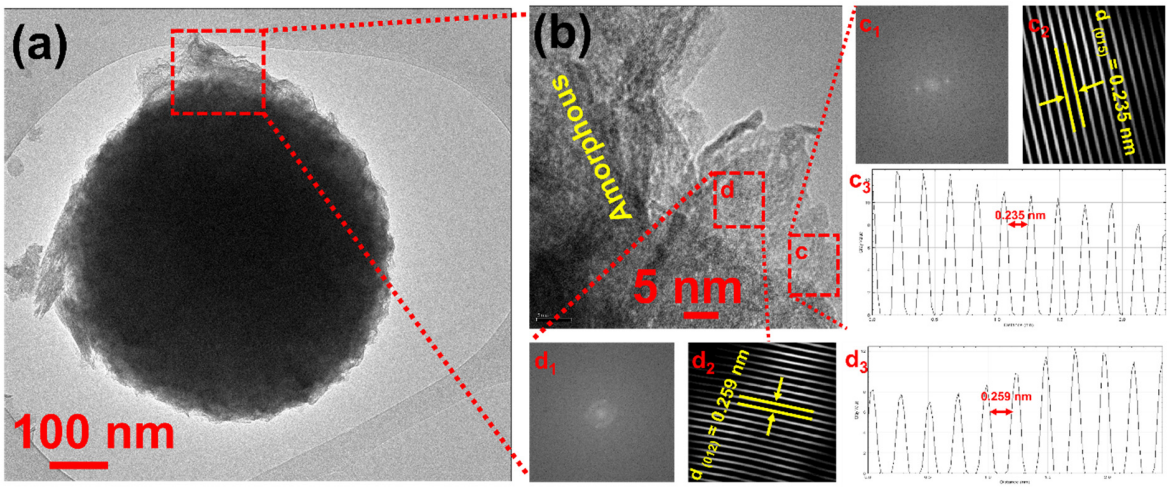

Figure S11: *Structural and morphology characterization of Ni_3Fe_2G sample after the stability test, (a) TEM image, (b) HRTEM image, the typical lattice fringes with a distance of 0.235 nm and 0,259 nm can be observed in HRTEM image in figure b (insert c_2 and d_2), which relates to the (015) and (012) facet of hexagonal NiFe* bimetallic glycerates *(JCPDS No:40-0216).*

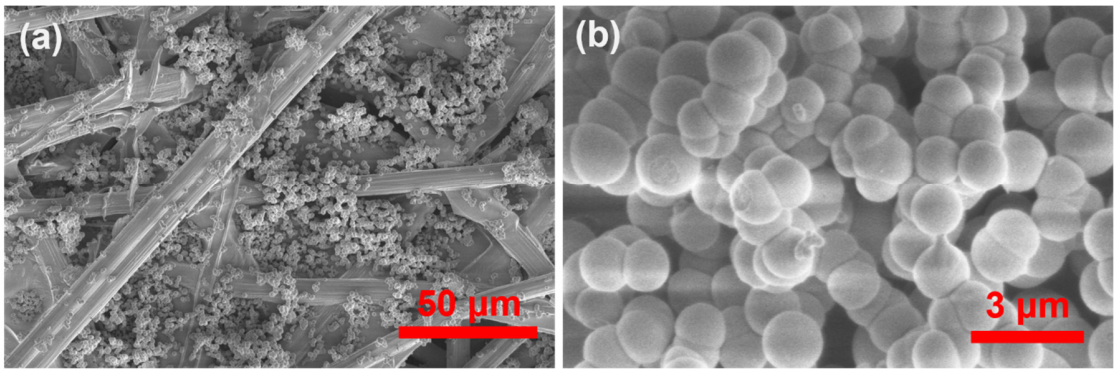

Figure S12: *Shows the SEM images of Ni_3Fe_2G microsphere after the stability test.*

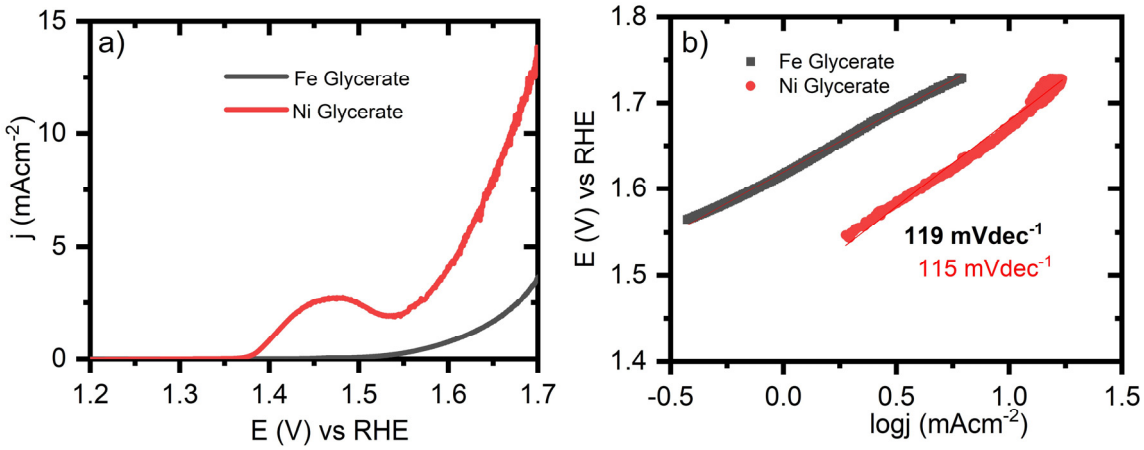

Figure S13: *a) Linear sweep voltammograms of Ni and Fe glycerates and b) their corresponding Tafel plots.*

Table S3: Comparison of the OER performance of various non-noble metal electrocatalysts.

Catalysts	**Electrolyte**	**Overpotential @ 10 mA cm^{-2} (mV)**	**Tafel slope (mV/dec)**	**Reference**
NiFeG	1 M KOH	320	74	This Work
NiFeG/CP	1M KOH	270 (50 mA cm^{-2})	-	This Work
NiFeOP	1 M KOH	310	43	[1]
FeNiG	1 M KOH	337 (50 mA cm^{-2})	75	[2]
FeCo-FeCoNi	1 M KOH	325	60	[3]
$Ni_{0.9}Fe_{0.1}$/NC	1 M KOH	330	45	[4]
$Ni_{70}Fe_{30}$ $(OH)_2$	1 M KOH	292	30	[5]
$Ni_{0.25}Cu_{0.75}$/C	1 M KOH	400	80	[6]
$Ni_{0.25}Co_{0.75}$ $(OH)_2$	1 M KOH	352	72	[7]

NiCoP /NF	1 M KOH	268	71	[8]
NiFeCr LDH	1 M KOH	280	130	[9]
NiFe-LDH/CNT	0.1M KOH	350	54	[10]
Ni-Fe-MoO_4-LDH	0.1M KOH	491	23	[11]
NiV-LDH/Ni Foam	1 M KOH	318	50	[12]

References:

1. Chen, J.; Guo, Z.; Luo, Y.; Cai, M.; Gong, Y.; Sun, S.; Li, Z.; Mao, C.-J. Engineering Amorphous Nickel Iron Oxyphosphide as a Highly Efficient Electrocatalyst toward Overall Water Splitting. *ACS Sustain. Chem. Eng.* **2021**, *9*, 9436–9443, doi:10.1021/acssuschemeng.1c02897.
2. Nguyen, T.X.; Su, Y.; Lin, C.; Ruan, J.; Ting, J. A New High Entropy Glycerate for High Performance Oxygen Evolution Reaction. *Adv. Sci.* **2021**, *8*, 2002446, doi:10.1002/advs.202002446.
3. Yang, Y.; Lin, Z.; Gao, S.; Su, J.; Lun, Z.; Xia, G.; Chen, J.; Zhang, R.; Chen, Q. Tuning Electronic Structures of Nonprecious Ternary Alloys Encapsulated in Graphene Layers for Optimizing Overall Water Splitting Activity. *ACS Catal.* **2017**, *7*, 469–479, doi:10.1021/acscatal.6b02573.
4. Zhang, X.; Xu, H.; Li, X.; Li, Y.; Yang, T.; Liang, Y. Facile Synthesis of Nickel–Iron/Nanocarbon Hybrids as Advanced Electrocatalysts for Efficient Water Splitting. *ACS Catal.* **2016**, *6*, 580–588, doi:10.1021/acscatal.5b02291.
5. Lee, E.; Park, A.-H.; Park, H.-U.; Kwon, Y.-U. Facile Sonochemical Synthesis of Amorphous NiFe-(Oxy)Hydroxide Nanoparticles as Superior Electrocatalysts for Oxygen Evolution Reaction. *Ultrason. Sonochem.* **2018**, *40*, 552–557, doi:10.1016/j.ultsonch.2017.07.048.
6. Ahsan, M.A.; Puente Santiago, A.R.; Hong, Y.; Zhang, N.; Cano, M.; Rodriguez-Castellon, E.; Echegoyen, L.; Sreenivasan, S.T.; Noveron, J.C. Tuning of Trifunctional NiCu Bimetallic Nanoparticles Confined in a Porous Carbon Network with Surface Composition and Local Structural Distortions for the Electrocatalytic Oxygen Reduction, Oxygen and Hydrogen Evolution Reactions. *J. Am. Chem. Soc.* **2020**, *142*, 14688–14701, doi:10.1021/jacs.0c06960.
7. Wang, Y.; Yang, C.; Huang, Y.; Li, Z.; Liang, Z.; Cao, G. Nickel Induced Electronic Structural Regulation of Cobalt Hydroxide for Enhanced Water Oxidation. *J. Mater. Chem. A* **2020**, *8*, 6699–6708, doi:10.1039/D0TA00010H.
8. Wang, J.-G.; Hua, W.; Li, M.; Liu, H.; Shao, M.; Wei, B. Structurally Engineered Hyperbranched NiCoP Arrays with Superior Electrocatalytic Activities toward Highly Efficient Overall Water Splitting. *ACS Appl. Mater. Interfaces* **2018**, *10*, 41237–41245, doi:10.1021/acsami.8b11576.

9. Yang, Y.; Dang, L.; Shearer, M.J.; Sheng, H.; Li, W.; Chen, J.; Xiao, P.; Zhang, Y.; Hamers, R.J.; Jin, S. Highly Active Trimetallic NiFeCr Layered Double Hydroxide Electrocatalysts for Oxygen Evolution Reaction. *Adv. Energy Mater.* **2018**, *8*, 1703189, doi:10.1002/aenm.201703189.
10. Gong, M.; Li, Y.; Wang, H.; Liang, Y.; Wu, J.Z.; Zhou, J.; Wang, J.; Regier, T.; Wei, F.; Dai, H. An Advanced Ni–Fe Layered Double Hydroxide Electrocatalyst for Water Oxidation. *J. Am. Chem. Soc.* **2013**, *135*, 8452–8455, doi:10.1021/ja4027715.
11. Nejati, K.; Davari, S.; Akbari, A.; Asadpour-Zeynali, K.; Rezvani, Z. A Highly Active Oxygen Evolution Electrocatalyst: Ni-Fe-Layered Double Hydroxide Intercalated with the Molybdate and Vanadate Anions. *Int. J. Hydrog. Energy* **2019**, *44*, 14842–14852, doi:10.1016/j.ijhydene.2019.04.045.
12. Fan, K.; Chen, H.; Ji, Y.; Huang, H.; Claesson, P.M.; Daniel, Q.; Philippe, B.; Rensmo, H.; Li, F.; Luo, Y.; et al. Nickel–Vanadium Monolayer Double Hydroxide for Efficient Electrochemical Water Oxidation. *Nat. Commun.* **2016**, *7*, 11981, doi:10.1038/ncomms11981.